where $(M/L)_{\text{N-R}}{}^0$ is the nonrelativistic Coulomb value for the M/L ratio. All terms that depend on the logarithm of the nuclear radius cancel out in the capture ratio. Equation (12) suggests that relativistic effects on $(M/L)^0$ are small for the values of Z listed in Table I. Using arguments of the kind given by Layzer and Bahcall,[18] one can see that relativistic corrections for $X^{M/L}$ are also of order $(\alpha Z)^2$ and, hence, small. The calculations of Band et al.[19] show that nuclear size effects on M/L ratios amount to less than 0.3% for Z less than 50. Hence, nuclear size effects can safely be neglected for Z less than 50.

IV. EXPERIMENTAL TEST. Ge^{71}

We have calculated the exchange-corrected M/L value for Ge^{71} using Eqs. (3) and Table I; we find[20]:

$$(M/L)_{\text{Th}} = 0.173, \tag{13}$$

[18] D. Layzer and J. Bahcall, Ann. Phys. (N. Y.) 17, 177 (1962).
[19] I. M. Band, L. N. Zyrianóva, and Tsin Chen-Zhui, Izv. Akad. Nauk SSSR Ser. Fiz. 20, 1389 (1956).
[20] The self-consistent field value of the M/L ratio without exchange is 0.151 and is not in disagreement with the results of Manduchi and Zannoni, although there are contrary statements in their papers (Ref. 10). The Hartree-Hartree wave functions

which is in good agreement with a similar calculation that we have performed using the somewhat less accurate wave functions of Hartree and Hartree.[17] Our theoretical prediction disagrees with the experimental result of Manduchi and Zannoni who obtained[10]:

$$(M/L)_{\text{Ex}} = 0.141 \pm 0.010. \tag{14}$$

It would be useful to perform other precision measurements of M/L ratios (e.g., for Zn^{65}, Ge^{71}, or Kr^{79}) in order to clarify this discrepancy between theory and experiment.

ACKNOWLEDGMENTS

(Ref. 17) and the Watson-Freeman wave functions (Ref. 8) both give $(M/L)^0 = 0.149$ for Ge^{71}.

Nuclear Reaction Energies with an Absolute Ion Velocity Gauge

B. R. Gasten*

University of Wisconsin, Madison, Wisconsin†

(Received 15 March 1963)

A time-of-flight technique was used to find the $Li^7(p,n)Be^7$ threshold energy and an $Al^{27}(p,\gamma)Si^{28}$ resonant energy. Results place the $Li^7(p,n)$ threshold at 1879.8±0.3 keV and the $Al^{27}(p,\gamma)$ resonance at 991.6±0.2 keV. The lithium threshold was determined by use of a (yield)$^{2/3}$ extrapolation. The aluminum resonant energy is taken as the half-height energy of a thick-target yield. Except for the earliest electrostatic analyzer results, there was good agreement with previous determinations of these energies. The proton beam was modulated at approximately 50 Mc/sec by use of an Einzel lens driven by a crystal controlled oscillator-amplifier at the ion source of an electrostatic accelerator. The time-of-flight equipment consisted of a drift tube of adjustable length, a "phase meter" employing a variable delay line, and two pickups consisting of tuned cylindrical tubes through which the proton beam passed. Frequency was measured by zero beating a variable-frequency crystal oscillator against the signal picked off the beam and counting the crystal frequency with a frequency counter standardized to WWV. The lithium and aluminum targets were protected from organic vapors by a concentric liquid nitrogen trap.

INTRODUCTION

THE present work was stimulated by an apparent systematic difference between absolute magnetic-deflection and absolute electric-deflection methods of measuring nuclear energies. Some of these earlier results are shown in Table I.

Very recent results (NRL,[1] 991.9±0.3, and Zurich,[2]

991.8±0.1) apparently remove the worst discrepancies. An absolute velocity device[3] used by Shoupp, Jennings, and Jones[4] at Westinghouse resulted in a threshold energy for the $Li(p,n)$ threshold which, perhaps unfortunately, overlapped the early electrostatic and magnetic-deflection results, thus giving no indication

[1] R. O. Bondelid and J. W. Butler (private communication).
[2] A. Rytz, H. H. Staub, and W. Zych, Helv. Phys. Acta 35, 341 (1962).

[3] W. Altar and M. Garbuny, Phys. Rev. 76, 496 (1949). A 1.25-m coaxial resonant cavity was excited at both ends by a 70-Mc/sec modulated proton beam. The center conductor was a field-free drift tube. The beam energy was varied to obtain minimum rf excitation when the transit time was an odd-multiple of half-cycles.
[4] W. E. Shoupp, B. Jennings, and W. Jones, Phys. Rev. 76, 502 (1949).

TABLE I. Al$^{27}(p,\gamma)$ and Li$^7(p,n)$ early results.

Group	Al$^{27}(p,\gamma)$ E_r(keV)	Li$^7(p,n)$ E_t(keV)	Method
Wisconsin$_1$[a]	993.3±1.0	1882.2±1.9	abs. electrostatic
Associated Electronics Industries[b]	993.5±0.8	...	abs. electrostatic
Naval Research Laboratory[c]	992.4±0.5	1881.2±0.9	abs. electrostatic
Rice[d]	992.2±0.5	1880.5±0.8	abs. magnetic
Zurich$_1$[e]	991.1±0.2	1880.3±0.5	abs. magnetic

[a] R. G. Herb, S. C. Snowdon, and O. Sala, Phys. Rev. 75, 246 (1949).
[b] S. E. Hunt, R. A. Pope, D. V. Freck, and W. W. Evans, Phys. Rev. 120, 1740 (1960).
[c] R. O. Bondelid and C. A. Kennedy, Phys. Rev. 115, 1601 (1959).
[d] E. H. Beckner, R. L. Bramblett, G. C. Phillips, and T. A. Eastwood, Phys. Rev. 123, 2100 (1961).
[e] H. H. Staub and H. Winkler, Nucl. Phys. 17, 271 (1960).

as to which of the determinations might contain a systematic deviation.

DESCRIPTION OF THE METHOD

The present paper reports more precise measurements from a somewhat different type[5] of absolute-velocity device. A schematic representation of the device is shown in Fig. 1. The proton beam was modulated at the ion source of the electrostatic accelerator at a stable frequency of 50 Mc/sec, was then accelerated to the desired energy, filtered of unwanted mass and energy components by the magnetic and electrostatic analyzers, and finally passed into the velocity determining equipment. Pickups were installed at two points along the path of the proton beam to allow the relative phase of the beam at these points to be determined. The distance between the pickups was variable. They were spaced at sufficient distance (approximately 2.4 m) that the protons took several periods (approximately 7) of the modulation to pass from one to the other. Small deviations from $n+\frac{1}{2}$ periods (n integer) were measured with a "phase meter" which consisted of a trombone type calibrated variable-
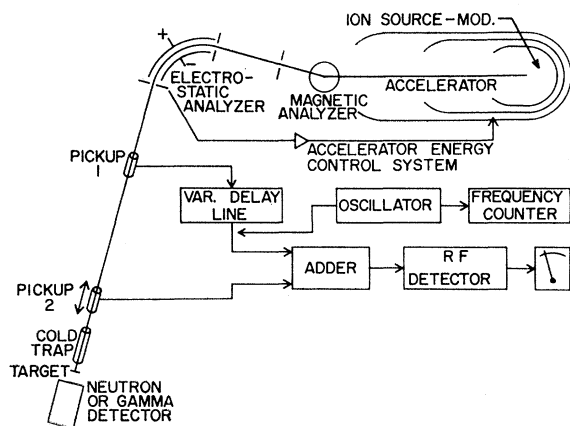
delay line, an adder, and a detector.[6] The time delay in one channel was varied until a minimum occurred in the output of the detector. There is, of course, an unknown time delay ϵ which results from uncertainties in the zero of the delay line, phase shifts in tuned circuits, etc. However, it is possible to eliminate ϵ by rotating the drift tube and pickups end for end. To demonstrate this we note that, because of ϵ, the distance d between pickups for a null will not be the same when the beam traverses the pickups in the opposite sense. However,

$$v=d_{12}[(n+\tfrac{1}{2})T+\tau_{12}+\epsilon]^{-1}=d_{21}[(n+\tfrac{1}{2})T-(\tau_{21}+\epsilon)]^{-1},$$

where τ is the delay introduced by the variable delay line (always in series with pickup 1), T, the period of modulation, and $n+\frac{1}{2}$ the number of wavelengths on the beam between the two pickups. The subscript 12 denotes passage of the beam from pickup 1 to pickup 2, and the subscript 21 passage from 2 to 1.

If v is approximately known (10%), then the integer n is easily fixed by $v\cong d[(n+\tfrac{1}{2})T]^{-1}$, which approximation is good for $\tau+\epsilon\ll T$.

Eliminating ϵ gives $v=(d_{12}+d_{21})[(2n+1)T+(\tau_1-\tau_2)]^{-1}$.

Since the relativistic corrections at the velocities of interest exceed 0.1%, the energy was calculated relativistically. The proton mass equivalent was taken as 938.219±0.010 MeV.

APPARATUS

Details of equipment and procedure are given in the Ph.D. thesis of the author[7] and, hence, are only briefly
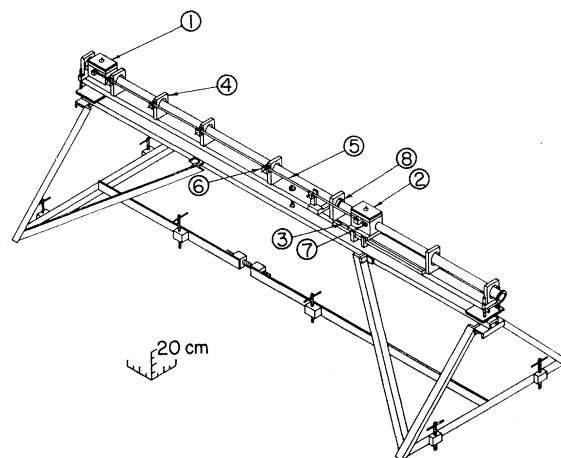

FIG. 1. Schematic diagram of entire system.

FIG. 2. Pickups and drift tube. Legend: (1) fixed pickup station; (2) movable pickup station; (3) track for movable pickup station; (4) adjustable drift-tube support; (5) Invar standard length bar; (6) adjustable support for Invar bar; (7) micrometer; (8) double O-ring telescoping joint.

[5] The method is rather similar to that used by J. H. Manley and M. J. Jacobson, Rev. Sci. Instr. 25, 368 (1954).
[6] The variable-delay line and adder, Phase Meter Model 205B, were supplied by Ad-Yu Electronics, Passaic, New Jersey, and to the author's knowledge constitute the only commercially available phase meter which operates at this frequency range with the desired accuracy.
[7] B. R. Gasten, Ph.D. thesis, University of Wisconsin, 1963 (Available from University Microfilms, Ann Arbor, Michigan).

described here. Nearly 100% modulation of the 50-Mc/sec beam was achieved by a 10-W crystal-controlled 25-Mc/sec supply driving an Einzel lens at the output of the ion source. Frequency stability was within 2 parts per million (ppm) during a day's run.

After acceleration by the electrostatic generator, the modulated beam passed through a 90° electrostatic analyzer preceding the time-of-flight device. The analyzer, with slits set for $\Delta E/E = 0.03\%$ served two functions: (1) Its high resolution improved the sharpness of the null detection; (2) While not used as an absolute-energy device, it served as a convenient short-time secondary energy reference for mapping resonant and threshold yields.

Figure 2 shows the drift tube with the two pickups, and Fig. 3 is a schematic view of one. The pickups consisted of tubes 9.78-cm long. They were connected through resonant transformers and transmission lines to the phase detector.

One of the pickups was permanently mounted on the drift tube, with the other on a movable truck which allowed the spacing between the pickups to be varied from 202 to 255 cm. The spacing was adjusted such that the signals nulled with the addition of a delay of less than 2 nsec to the signal from the fixed pickup.

A block diagram of the electronics involved in the determination of velocity is depicted in Fig. 4. The bandwidth of the receiver system was adjusted to 1.2 kc/sec with a crystal filter.

Although the position of the nulls was taken manually for all the data used in the experiment, several runs were made using a motor drive on the variable delay line and an oscillograph attached to the output of the receiver system. One of the resulting curves is shown in Fig. 5. Drifts in the gain and tuning of the receiver system and slow changes in beam current give asymmetries in the curves. Rapid fluctuations of beam current make the curve rather ragged.
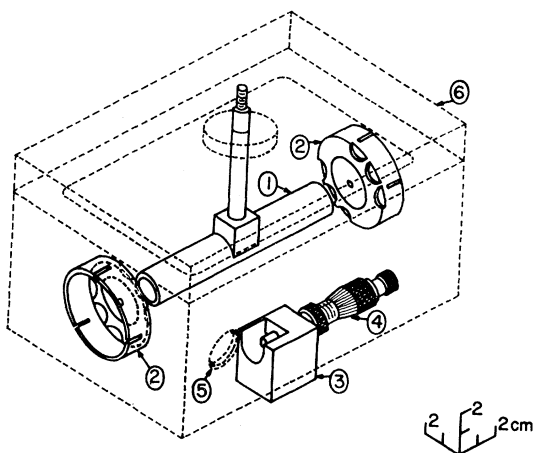

FIG. 3. Detail of movable pickup station. Legend: (1) pickup tube; (2) collimator assembly; (3) end support for Invar bar; (4) micrometer; (5) alignment hole; (6) Lucite cover plate. (A brass plate carrying the resonant circuit mounts on top of 6.)
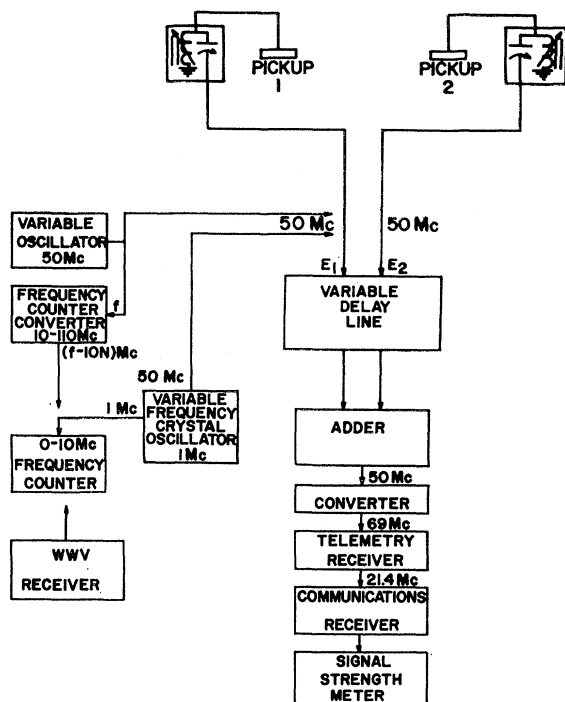

FIG. 4. Block diagram of electronics associated with pickup system. The equipment on the left of the figure is associated with the determination of the beam-modulation frequency.

To measure the frequency of modulation of the beam, the 50-Mc/sec output of an adjustable-frequency crystal oscillator was adjusted to zero beat with the detected modulation on the beam. The 1-Mc/sec output of this oscillator was counted on a frequency counter standardized to WWV.

After passing through the pickups the proton beam entered the target system, shown in Fig. 6. The target was protected from contaminants by the concentric liquid-nitrogen trap. Secondary emission from the target and collimator was suppressed with 1900-V negative applied to the suppressor cylinder between the target and collimator.

Targets of lithium or aluminum metal were evaporated in vacuum onto 0.04-cm thick tantalum disks, and then exposed for several hours to dry oxygen before
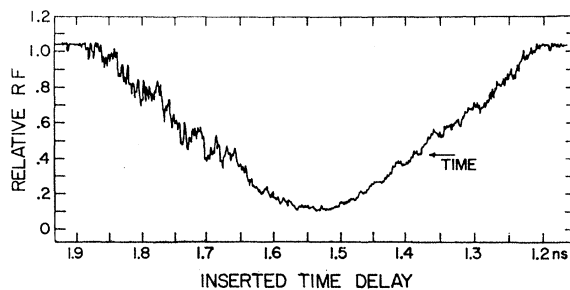

FIG. 5. Output of phase detector as the variable delay was mechanically increased at the rate of ~0.2 nsec/min.
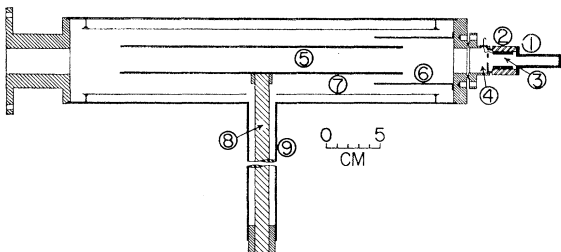
Fig. 6. Cold trap and target system. Legend: (1) target cup; (2) ceramic insulator; (3) suppressor electrode; (4) collimator; (5) concentric liquid-nitrogen cooled trap; (6) baffle; (7) radiation shield; (8) copper heat conductor; (9) stainless steel finger. An aluminum gasket is used to join the trap and the target system.

removal from the evaporator. They were stored in a desiccator jar prior to use. To minimize contamination a separate target was used each day. After evacuation they were maintained at approximately 150°C prior to use, and were not kept in a vacuum for longer than 16 h prior to use.

For the $Li^7(p,n)Be^7$ neutron threshold a long counter of the type described by Hanson and McKibben[8] was used. A 6342A photomultiplier with a 5-cm×5-cm sodium iodide crystal was used for the $Al^{27}(p,\gamma)Si^{28}$ resonance.

EXPERIMENTAL PROCEDURE

After warmup of the accelerator and associated equipment, the modulated proton beam was optimized for maximum current consistent with high rf modula-
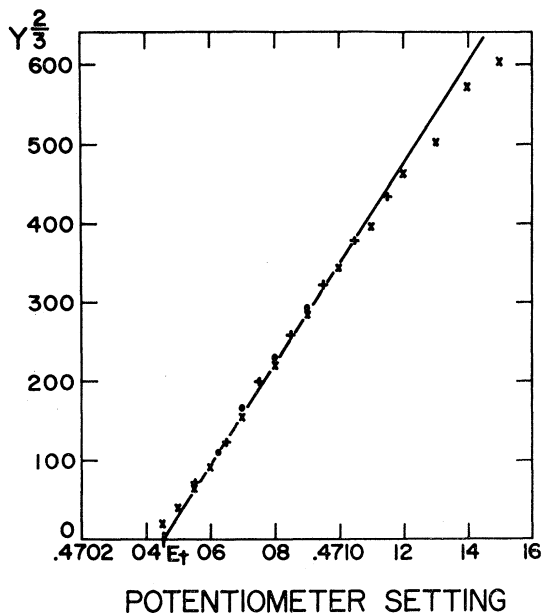

Fig. 7. Neutron yield from $Li^7(p,n)$ reaction near threshold. (Yield)$^{2/3}$ versus potentiometer setting of electrostatic analyzer defining beam energy. Different symbols indicate different consecutive runs over curve. The symbol size is greater than or equal to statistical uncertainties.

[8] A. O. Hanson and J. L. McKibben, Phys. Rev. 72, 673 (1947).

tion. Normal beam current at target was of the order of 0.5 μA.

Thick-target yield curves were obtained as a function of electrostatic-analyzer voltage for the reaction under study. Because the cross section for s-wave neutron production goes as $(\Delta E)^{1/2}$ immediately above threshold, the yield from a thick target should go as the integral of this, namely $Y \propto (\Delta E)^{3/2}$. Hence, the plot of $Y^{2/3}$ versus proton energy should be linear in the region just above threshold.

The yield curve was repeated a number of times until the electrostatic-analyzer potentiometer setting corresponding to the extrapolated threshold stabilized. The time-of-flight equipment was then used to determine the velocity of the proton beam corresponding to this setting.

The first step in the velocity determination was to move the second pickup until the rf minimum was within the 0- to 2-nsec range of the variable delay line.

The phase difference between the two pickups was then found by the following procedure. The phase-detector gain controls were adjusted so that the two pickup signals were of the same amplitudes. The variable delay line was then adjusted to obtain a minimum in rf output. To achieve reproducible minima, large fluctuations of beam current or focus had to be avoided.

This search for minimum rf was repeated at least ten times and the corresponding delay-line readings recorded. The electrostatic analyzer was then rebalanced, and the focus of the accelerator readjusted to reduce drifts, prior to another set of at least ten null readings. In total, at least four sets of at least ten nulls were taken. The frequency of modulation on the proton beam was determined, with at least ten separate determinations being made.

The drift tube including pickups and associated leads were then rotated end for end and the entire procedure outlined above was repeated.

Finally, the threshold-energy yield curves in terms of electrostatic-analyzer setting were repeated to measure possible drift during the period of velocity determination.

The same general procedure was used for the $Al^{27}(p,\gamma)Si^{28}$ thick-target yield curves. The velocity determination was made at the potentiometer setting corresponding to the half-height of the thick-target yield curve.

A CDC-1604 computer was programmed for reducing the data to velocities and energies and for computing standard deviations.

RESULTS

In the final $Li^7(p,n)Be^7$ data, eight velocities were measured, each corresponding to an extrapolated threshold of a fresh lithium target. A typical curve is given in Fig. 7. The extrapolated thresholds were taken as the best visual fit to the linear portion of the curve.
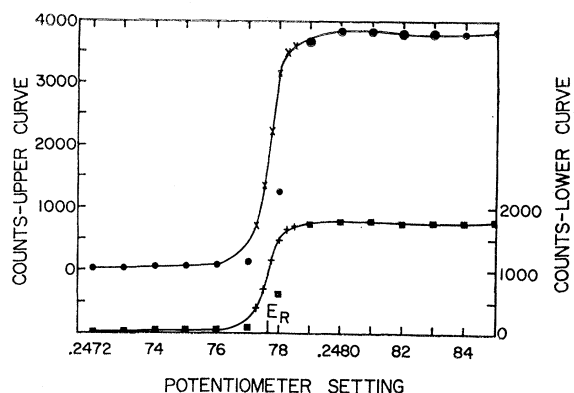
FIG. 8. Gamma-ray yield from $Al^{27}(p,\gamma)$ reaction from thick target. Yield versus potentiometer setting of electrostatic analyzer defining beam energy. The upper curve results from counting gammas of all energies. The lower curve results from counting only gammas of energy ≥ 9 MeV. Different symbols indicate different consecutive runs over the curve. The closed circles were determined simultaneously with the closed squares, and the ✕'s were determined simultaneously with the (✛)'s. The symbol size exceeds or equals the statistical uncertainties. An example of analyzer drift is shown in the displacement of the closed symbols from the step in the curve.

Similarly, eight velocity determinations were made for the $Al(p,\gamma)$ resonance. A typical thick-target curve for the aluminum resonance is given in Fig. 8. The lower of the two curves results from counting only gammas of energy ≥ 9 MeV, while the upper is the result of counting gammas of all energies.

The average threshold or resonant energy quoted in Tables II and III was obtained by means of a weighted average of the results of the eight individual determinations. The weighting factor used was the reciprocal of the sum of the squares of those uncertainties unique to each individual run. These included uncertainties in energy due to analyzer drift, and in the determination of the rf minimum.

TABLE II. $Li^7(p,n)Be^7$.

Group	ϵ_{th} (keV)	Method
Wisconsin$_1$[a]	1882.2 ±1.9	Abs. electrostatic
Naval Research Laboratory[b]	1881.2 ±0.9	Abs. electrostatic
Rice[c]	1880.5 ±0.8	Abs. magnetic
Zurich$_2$[d]	1880.48±0.25	Abs. magnetic
Zurich$_1$[e]	1880.3 ±0.5	Abs. magnetic
Westinghouse[f]	1881.2 ±1.9	Abs. velocity
Wisconsin$_2$[g]	1879.7 ±1.1	$Ni^{60}\gamma$, 1.3325
Wisconsin$_2$[h]	1879.4 ±1.0	$Hg^{198}\gamma$, 0.411770
Present	1879.8 ±0.3	Abs. velocity

[a] R. G. Herb, S. C. Snowdon, and O. Sala, Phys. Rev. 75, 246 (1949).
[b] R. O. Bondelid and C. A. Kennedy, Phys. Rev. 115, 1601 (1959).
[c] E. H. Beckner, R. L. Bramblett, G. C. Phillips, and T. A. Eastwood, Phys. Rev. 123, 2100 (1961).
[d] A. Rytz, H. H. Staub, and H. Winkler, Helv. Phys. Acta. 34, 960 (1961).
[e] H. H. Staub and H. Winkler, Nucl. Phys. 17, 271 (1960).
[f] See Ref. 4.
[g] K. W. Jones, R. A. Doublas, M. T. McEllistrem, and H. T. Richards, Phys. Rev. 94, 947 (1954).
[h] Ref. g, as corrected for new value of Mg^{24} first excited state determined by Murray et al. [G. Murray, R. L. Graham, and J. S. Geiger, Bull. Am. Phys. Soc. 7, 72 (1962).]

TABLE III. $Al^{27}(p,\gamma)Si^{28}$.

Group	ϵ_{th} (keV)	Method
Assoc. Elec. Ind.[a]	993.5±0.8	Abs. electrostatic
Wisconsin[b]	993.3±1.0	Abs. electrostatic
Naval Research Laboratory[c]	991.9±0.3	Abs. electrostatic
Rice[d]	992.2±0.5	Abs. magnetic
Zurich$_2$[e]	991.8±0.1	Abs. magnetic
Zurich$_1$[f]	991.1±0.2	Abs. magnetic
Present	991.6±0.2	Abs. velocity

[a] S. E. Hunt, R. A. Pope, D. V. Freck, and W. W. Evans, Phys. Rev. 120, 1740 (1960).
[b] R. G. Herb, S. C. Snowdon, and O. Sala, Phys. Rev. 75, 246 (1949).
[c] See Ref. 1.
[d] E. H. Beckner, R. L. Bramblett, G. C. Phillips, and T. A. Eastwood, Phys. Rev. 123, 2100 (1961).
[e] See Ref. 2.
[f] H. H. Staub and H. Winkler, Nucl. Phys. 17, 271 (1960).

No corrections have been made for the Lewis effect.[9] Therefore, the present values are directly comparable to older measurements. Detailed calculations will be necessary to assess the magnitude of the effect for our particular arrangement. However, preliminary calculations based upon the recent work of Palmer et al.[10] suggests a shift of about 80 V upwards for the $Al(p,\gamma)$ resonance, and perhaps 200 V upward for the $Li^7(p,n)$ threshold.

ERROR ANALYSIS

The major errors which can be anticipated may be grouped under three categories which are (1) uncertainties in length, (2) uncertainties in frequency, and (3) uncertainties in phase. They will be discussed in this order. Table IV lists the uncertainties along with their magnitudes.

TABLE IV. Uncertainties.

	% energy✕ (10^{-3})	
Length		
Invar bars	3.2	
Position of bars relative to pickups	7.0	
Pickup tolerance	4.4	
End effects	7.6	
Skewness	4.4	
Magnetic Fields	0.01	
Temperature	1.0	
Length subtotal, rms	12.5	
Frequency		
Error in frequency counter	0.2	
Error in beat	0.4	
Phase	$Al^{27}(p,\gamma)$	$Li^7(p,n)$
Calibration of delay line	6.0	16.0
Drift and null uncertainty	15.2	25.0
Total error, rms	20.6	32.2

[9] H. W. Lewis, Phys. Rev. 125, 937 (1962); W. L. Walters, D. G. Costello, J. G. Skofronick, D. W. Palmer, W. E. Kane, and R. G. Herb, Phys. Rev. Letters 7, 284 (1961).
[10] D. W. Palmer, J. G. Skofronick, D. G. Costello, A. L. Morsell, W. E. Kane, and R. G. Herb (unpublished).

The Invar bars were each calibrated by the National Bureau of Standards to within 0.0015 cm.

The error in adjusting the pickups against the alignment bar is estimated to be less than 0.0015 cm for each. The adjustment of the Invar support bracket against the alignment bar should not result in an uncertainty greater than 0.0015 cm. The micrometer head is adjusted to zero against the alignment bar to within 0.0005 cm. An uncertainty of 0.004 cm is assumed because of the possibility of nonintimate contact between the Invar bars against each other and against the stop and micrometer. The sum of these uncertainties is then 0.008 cm.

The pickups were carefully measured and their lengths differed by 0.013 cm. This difference was in the direction to cause the measured length to be less than the real length by 0.006 cm, with an uncertainty of 0.0025 cm. This correction (called "pickup tolerance" in Table IV) has been applied to all appropriate length measurements.

The electrical connection to the pickup not being in the center will result only in a contribution to ϵ.

In estimating the uncertainty in the effective positions of the pickups possible asymmetries in electrical end effects must be considered. A conservative estimation of this asymmetry was made by assuming that the effective end of the pickup could be half way between the real end and the grounded collimator plate at the wall of the box. The result would be a net displacement of 0.009 cm, corresponding to the velocity being 0.0038% higher than measured. This correction has not been made but is included as an uncertainty.

Beam collimators guarantee that the skewness of the beam with respect to the measuring rods cannot exceed 0.048 cm in 2.4 m. Magnetic-field effects (measured to be ≤ 0.9 G) result in a negligible uncertainty. Temperature variations were always less than $\pm 3°C$ and have contributed an uncertainty of $\leq 5 \times 10^{-4}\%$ to the length.

The total rms error in length due to the above indicated uncertainties is $6.26 \times 10^{-3}\%$, corresponding to an rms uncertainty in energy of $12.5 \times 10^{-3}\%$.

The error in the calibration of the frequency counter against WWV was never found to be more than 10 cycles in 10 Mc/sec, corresponding to negligible uncertainty in energy. The uncertainty in the determining of zero beat between the variable-frequency crystal oscillator and the modulation on the beam is estimated to be less than 2×10^{-6}, or $4.0 \times 10^{-4}\%$ in energy. Any instability of modulation frequency was masked by the uncertainty of determining zero beat.

Phase errors due to random changes in beam conditions are included in "Drift and null uncertainty" in Table IV. The variable delay line was calibrated by inserting a fixed delay corresponding to several periods in series with one of the inputs to the adder. The input signal frequency from a signal generator was adjusted to some value near 50 Mc/sec such that null occurred in the output of the adder when this signal was connected to both inputs. The frequency was then changed slightly and the variable delay line readjusted to obtain a null. Knowing the number of periods in the fixed delay and the precise frequency, one can determine the exact increment of time change in the variable delay line. This procedure was repeated until the entire delay line was calibrated. The uncertainty in the calibration of the phase meter was less than 0.02 nsec for the lithium determinations, and about 0.01 nsec for the aluminum determinations.

The drift of the electrostatic analyzer during the period of a run was determined as indicated earlier. The uncertainty caused by drift is included under "Drift and null uncertainty" in Table IV.

The preceding estimates of uncertainties are presented in Table IV, along with the total uncertainties, which are taken as the square root of the sum of the squares, for both aluminum and lithium.

CONCLUSIONS

The results of the present work as well as the results of other groups are presented in Tables II and III. There are a number of differences larger than the estimated uncertainties. In fact, there is still some suggestion of differences systematic to a particular technique of measuring nuclear standards.

With a more stable accelerator, it may be possible to obtain results with appreciably smaller uncertainties. Higher frequencies and longer drift tube could improve the precision. Further lessening of the uncertainties would result from higher precision in the construction of the pickups, particularly with respect to their being identical. Modifications of technique in more detail are suggested in the Ph.D. thesis of the author.[7]

ACKNOWLEDGMENTS